Temperature-Dependent Electronic and Vibrational Structure of the 1-Ethyl-3-methylimidazolium Bis(trifluoromethylsulfonyl)amide Room-Temperature Ionic Liquid Surface: A Study with XPS, UPS, MIES, and HREELS†

S. Krischok,*,‡ M. Eremtchenko,‡,|| M. Himmerlich,‡ P. Lorenz,‡ J. Uhlig,‡ A. Neumann,‡ R. Öttking,‡ W. J. D. Beenken,‡ O. Höfft,§ S. Bahr,§ V. Kempter,§ and J. A. Schaefer‡

Institut für Physik and Institut für Mikro- und Nanotechnologien, Technische Universität Ilmenau, P.O. Box 100565, D-98684 Ilmenau, Germany, and Institut für Physik und Physikalische Technologien, Technische Universität Clausthal, Leibnizstr. 4, D-38678 Clausthal-Zellerfeld, Germany

Received: October 30, 2006; In Final Form: March 3, 2007

The near-surface structure of the room-temperature ionic liquid 1-ethyl-3-methylimidazolium bis(trifluoromethylsulfonyl)amide has been investigated as a function of temperature between 100 and 620 K. We used a combination of photoelectron spectroscopies (XPS and UPS), metastable induced electron spectroscopy (MIES), and high-resolution electron energy loss spectroscopy (HREELS). The valence band and HREELS spectra are interpreted on the basis of density functional theory (DFT) calculations. At room temperature, the most pronounced structures in the HREELS, UPS, and MIES spectra are related to the CF_3 group in the anion. Spectral changes observed at 100 K are interpreted as a change of the molecular orientation at the outermost surface, when the temperature is lowered. At elevated temperatures, early volatilization, starting at 350 K, is observed under reduced pressure.

1. Introduction

Room-temperature ionic liquids (RT-ILs) have attracted much attention for their excellent properties, namely they remain in liquid phase over a wide temperature range, have very low vapor pressure at RT, are chemically inert, and possess high heat capacities.[1,2] These properties make them good candidates for use in many fields.[2,3] They may be used as "green" solvents,[2] heat reservoirs,[4] as well as electrolytes in electrochemical applications,[5] homogeneous catalysis,[2,6,7] and dye sensitized solar cells.[8] In order to refine the performance of RT-ILs, detailed knowledge of the geometric, electronic, and vibrational structure of RT-ILs as a function of temperature appears indispensable. The need for vacuum-based studies employing surface analytical techniques has been pointed out recently.[9] So far, only a few of these studies have appeared very recently.[1,10−15]

A typical representative of RT-ILs is 1-ethyl-3-methylimidazolium bis(trifluoromethylsulfonyl)amide ([EMIM][Tf_2N]).[16,17] In two previous studies, we have applied ultraviolet and X-ray photoelectron spectroscopy (UPS (He I and II), XPS) as well as metastable induced electron spectroscopy (MIES),[13] partially supported by density functional theory (DFT) calculations,[14] to the study of the electronic structure of [EMIM][Tf_2N] at room temperature. In the present study, we have investigated the surface-near structure using the above-mentioned techniques as a function of temperature. In addition, we report the temperature- and depth-dependence of the vibrational spectrum for the [EMIM][Tf_2N] film at 100 and 300 K as measured with high-resolution electron energy loss spectroscopy (HREELS). We utilize quantum-chemical calculations based on DFT in order to analyze the electronic and vibrational spectra.

† Part of the special issue "Physical Chemistry of Ionic Liquids".

* Corresponding author. Tel.: +49-3677-69-3405. Fax: +49-3677-69-3365. E-mail address: stefan.krischok@tu-ilmenau.de.

‡ Technische Universität Ilmenau.

§ Technische Universität Clausthal.

|| Deceased.

2. Experimental and Theoretical Methods

2.1. Sample Preparation. A polycrystalline Au film of ∼250 nm thickness deposited on Si(100), separated by a Ti adhesion layer, serves as sample support. The samples were prepared by depositing one droplet of the ultrapure RT-IL onto the Au substrate, and were, after careful outgassing in a load lock system, introduced into the UHV chamber. The prepared [EMIM][Tf_2N] samples have very low vapor pressure, and no change of the base pressure could be detected during the measurements performed at RT. After the introduction of the RT-IL into the UHV chamber, the samples were characterized by XPS. The survey spectra indicate that a closed RT-IL film was successfully prepared. From the absence of any substrate (Au) related spectral feature in the XPS spectra, we estimate a film thickness of more than 10 nm.

Since the ionic liquid can be damaged by photons and electrons, special attention has been paid to minimize the irradiation time. In both the HREELS and the combined MIES/UPS measurements, the applied flux was kept rather low. Moreover, we have carefully checked that the spectra taken after warming up to RT are virtually identical to the original data obtained at RT. Thus, we tend to exclude beam damage to be responsible for the observed spectral changes. Auxiliary experiments show that metastable atoms, low-energy photons, and electrons with an kinetic energy of ∼10 eV cause, in contrast to high-energy photons and electrons (>1keV), only minor changes in the valence band and vibrational spectra, even if comparably high fluxes are applied.

2.2. Experimental Methods. This study is a continuation of our previous activities.[13,14] Briefly, it combines photoelectron spectroscopy (ultraviolet photoelectron spectroscopy, UPS (He I and II) and monochromated X-ray photoelectron spectroscopy, XPS (Al Kα)), metastable induced electron spectroscopy (MIES), and high-resolution electron energy loss spectroscopy (HREELS) performed in different UHV systems (base pressure

10.1021/jp067136p CCC: $37.00
Published on Web 05/03/2007

below 2×10^{-10} Torr). All chambers are equipped with a LN_2-cooling system enabling measurements down to approximately 100 K. Our monochromated XPS measurements feature an energy resolution below 0.6 eV ($Ag(3d_{5/2})$ at 15 eV pass energy), whereas a resolution below 250 meV was employed for all UPS and MIES measurements presented here. For HREELS a Delta 0.5 spectrometer (Ibach type) was applied, having an intrinsic energy resolution of $\sim$40 cm^{-1} (5 meV) for the device settings used in the presented experiments. A more detailed introduction into the experimental setups can be found elsewhere.[13,14]

Special attention must be paid to avoid charge-up effects, well-known for inorganic salts, during the application of any electron spectroscopies. For this reason, the probe beam currents were chosen low enough to avoid features attributable to typical charging phenomena (see below). Special care is required when performing measurements at reduced temperatures where the conductivity of the IL is reduced drastically (see sections 3.1 and 3.2).

2.3. DFT Calculations. In order to interpret the experimental results, we have performed electronic structure and vibrational frequency calculations for an [EMIM][Tf_2N] ion pair as well as for the individual ions using DFT as implemented in Gaussian 03.[18] We utilized Becke's B3LYP functional[19] and a 6-311G basis set with (3d, 2pd) polarization functions. We analyze the molecular Kohn−Sham orbitals of all states contributing to the electronic density of states (DOS) in the energy range accessible to UPS and MIES. Though Koopman's theorem is not valid for DFT, the DOS of occupied molecular states, as measured by UPS and MIES, is well determined for Janak's theorem[20] and the hybrid character of the B3LYP functional, which partially includes the Hartree−Fock exchange term.[21−24]

In order to simulate the HREELS spectra both IR-dipoles and Raman-activities for the electronic ground state are calculated. Here we analyzed the respective normal modes. Details to selection rules may be found in ref 25.

3. Results

3.1. Core Level Spectra (XPS). In Figure 1, the C(1s) and N(1s) emission as observed by XPS are presented as a function of temperature. At room temperature, the C(1s), N(1s), O(1s), F(1s), and S(2s) emissions display well-resolved and narrow spectral features. Neither emission from the substrate nor from unexpected elements could be detected. Furthermore, the relative peak areas agree well with the stoichiometry of the molecule. It is important to note that the data presented in Figure 1 have been taken under rising temperature. From the similarity of the RT spectrum with spectra directly taken at RT after introducing the film into UHV (see ref 13), we conclude that even in the presented XPS spectra beam damage plays a minor role. A detailed discussion of the XPS spectra typical for the [EMIM]-[Tf_2N] film at room temperature can be found elsewhere.[13] At lower temperatures, the following changes in the spectra are observed. Between 200 K and room temperature, the structures are narrow and no significant change in their line width is registered, whereas at temperatures between 150 and 200 K, a broadening of all core level peaks is observed, which prevents the separation of the different chemical states (see Figure 1). Furthermore, a reduction of the kinetic energy of all core levels toward lower values is observed at low temperatures (up to 10 eV at 120 K).

We attribute this behavior to charging of the sample surface due to a reduction of the IL film conductivity when lowering the temperature.[12,26] As an example, the behavior of [EMIM] $EtSO_4$ during cooling below the solidification point has been studied with XPS and TOF−SIMS.[12] Upon solidification, the material behaved as an electrical insulator, and charge compensation was required to allow for spectra to be recorded. In this context, it should be further mentioned that the [EMIM][Tf_2N] undergoes a phase transition in the investigated temperature range.[27]

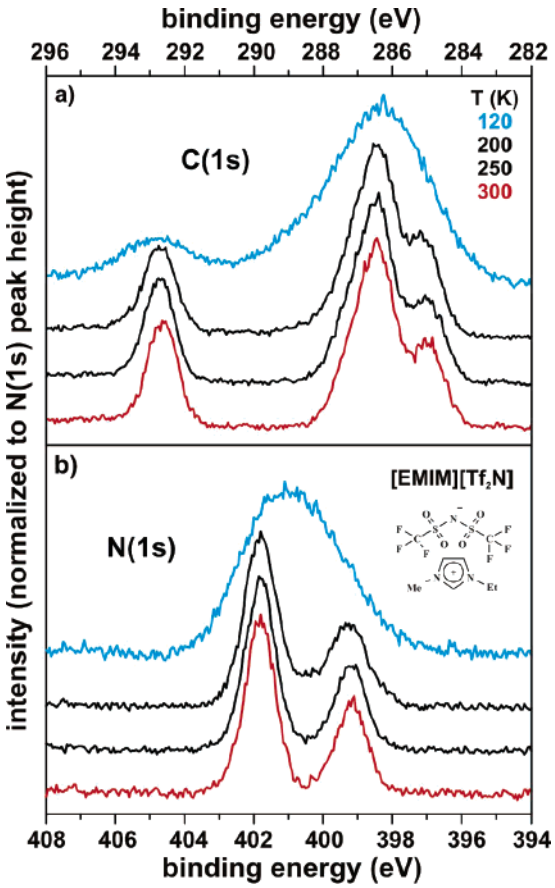

Figure 1. Temperature dependence of the [EMIM][Tf_2N] core level spectra upon cooling measured using monochromated Al Kα radiation; (a) C(1s) and (b) N(1s). For visualization the spectra are displayed in binding energy, where the position of the spectra was shifted to the energy observed at 300 K.

3.2. Valence Band Spectra (UPS, MIES). Room-temperature valence band spectra of [EMIM][Tf_2N] obtained using various electron spectroscopy techniques can be found in refs 13 and 14. Upon variation of information depth using different excitation sources, no significant spectral changes can be observed.[14]

At low temperatures, strong changes in the MIES and UPS spectra are observed. The changes of the valence band spectra occurring during temperature reduction to 127 K were reported by us in ref 13. In contrast to our XPS measurements, we tend to exclude charging during the application of MIES and UPS (with low intensities as provided by our MIES/UPS-source), because low intensities of the probe beams are employed. Furthermore, none of the features typical for charging are observed. In particular, no shift of any of the spectral features occurs nor do they become smeared out. Furthermore, a continuous decrease of the onset of the spectra at low kinetic energies would be seen, which is not the case. Nevertheless, we will base our discussion of the low temperature behavior mainly on our HREELS results in combination with DFT calculations.

The MIES and UPS results from annealing the film up to 620 K are presented in Figure 2. Above $\sim$350 K, the spectra change with increasing temperature. We notice an intensity decrease of the double peak at $\sim$11 eV. Additionally, together

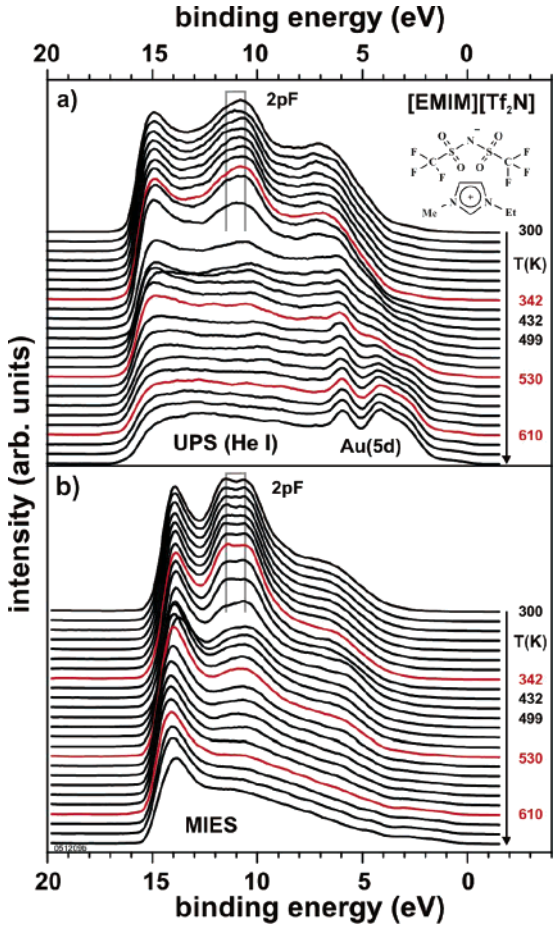

Figure 2. Temperature dependence of the valence band upon heating measured using (a) UPS (He I) and (b) MIES.

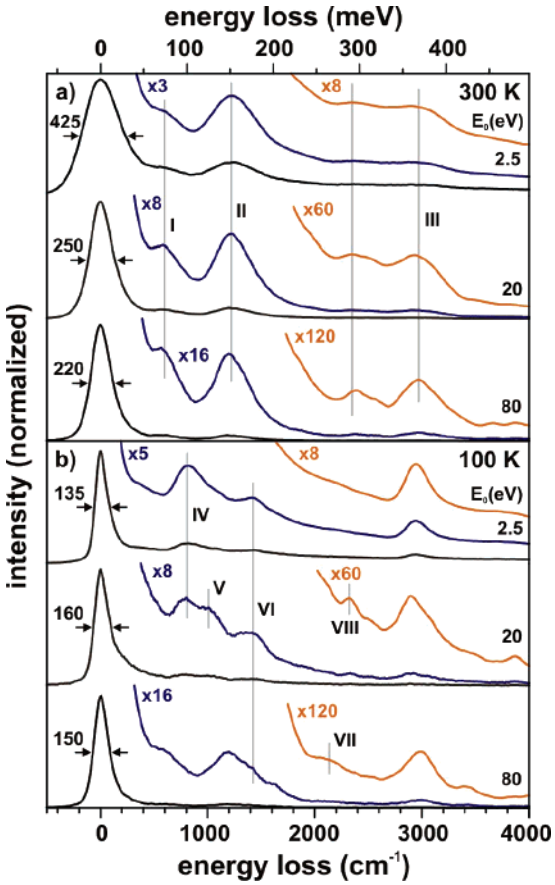

Figure 3. HREELS spectra of [EMIM][Tf_2N] at (a) 300 K and (b) 100 K using different primary beam energies. The magnified spectra have been subject to a smoothing procedure for better visibility of the features.

with the disappearance of the structure at ~11 eV, the structure at ~6 eV changes, too.

Above 500 K, the broad structure in UPS, centered around 7 eV, loses intensity and three sharp features at ~6, ~4, and ~3 eV, respectively, start to grow continuously with increasing temperature. These structures are well-known for an Au surface. In the same temperature range, the structures typical for [EMIM]-[Tf_2N] disappear in MIES, and the spectra become structureless. The observed MIES spectra are typical for a high work function metal such as Au.

3.3. Vibrational Spectra (HREELS). In order to get more information on eventual structural changes occurring during cooling, we have applied vibrational spectroscopy. In Figure 3, HREELS spectra of [EMIM][Tf_2N] are shown at 300 and 100 K sample temperature, respectively. For both temperatures, spectra were collected at different primary beam energies E_0 (2.5, 20, and 80 eV). At room temperature (Figure 3a), besides the elastic peak, loss structures are visible at ~580 cm^{-1} (marked as I in Figure 3), ~1200 cm^{-1} (II), ~2400 cm^{-1} (2 × 1200 cm^{-1}), and ~2980 cm^{-1} (III) in the investigated spectral range (0−4000 cm^{-1}). These main features are clearly visible for all used primary electron energies. Some less pronounced and not as well resolved structures (e.g. at 1400 , 2500, and 3100 cm^{-1}) are present in the spectra, too. The observed FWHM of the elastic peak decreases from 425 cm^{-1} for a primary beam energy of E_0 = 2.5 eV to 220 cm^{-1} for E_0 = 80 eV. Notably, the resolution of the applied device settings (40 cm^{-1}) is much better than the observed width of the elastic peak.

At 100 K, the spectra show characteristic changes as compared to the room temperature measurements (see Figure 3). All peaks, the elastic and all observed loss features, narrow. However, they are still considerably wider than the intrinsic resolution of the apparatus. The observed changes of the width of the elastic peak (FWHM) with primary beam energy (135 cm^{-1} at E_0 = 2.5 eV and 160 cm^{-1} at E_0 = 20 eV) are less pronounced. The observed loss structures at 100 K are more complex compared to the spectra taken at 300 K, and the spectra now change drastically with beam energy. Compared to the HREELS spectra at 300 K, in the spectra at 100 K additional loss structures at 810 (IV), 990 (V), 1430 (VI), 2120 (VII), and 2350 cm^{-1} (VIII) are now visible. These new features are most pronounced for low primary beam energies. With increasing primary beam energy the spectra start to resemble those for 300 K.

3.4. Electronic DOS Obtained by DFT. For the interpretation of the valence band spectra, we employ quantum-chemical DFT calculations of the electronic DOS for the single ions $[EMIM]^+$ and $[Tf_2N]^-$ as well as for the [EMIM][Tf_2N] ion pair complex. A detailed analysis of the corresponding Kohn−Sham molecular orbitals (MO) has been made previously.[14] In Figure 4a, the total electronic DOS is compared with the UPS and MIES measurements carried out at RT. For optimal comparison with experiment, a Gaussian broadening of 0.8 eV (FWHM) and a shift of 1.35 eV toward lower binding energies was applied to the DOS. Good qualitative agreement exists with the energetic positions of most features seen in the spectra (except for the spectral region around 14 eV, which is strongly influenced by secondary electron emission). A quantitative fit of the shape of the spectra cannot be expected because the

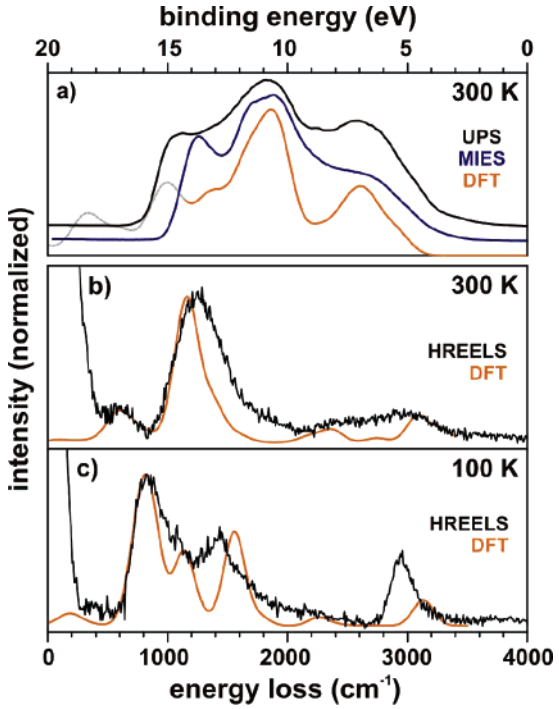

Figure 4. (a) MIES and UPS (He I) measurements of [EMIM][Tf_2N] at 300 K compared to DFT calculations of the total density of occupied states. (b) Background-corrected HREELS spectrum at 300 K (primary electron beam energy $E_0 = 2.5$ eV) compared to the vibrational calculations of the gas-phase ion pair. (c) Low temperature HREELS spectrum ($T = 100$ K, $E_0 = 2.5$ eV) compared to vibrational modes possessing dipole activities perpendicular to the central $[EMIM]^+$ ring (for details see text).

intensities of the different spectroscopic methods do not depend on the DOS only.

As previously,[14] we find that all states from the highest occupied state at 6.7 eV (5.3 eV including shift) down to those of a binding energy of 9.0 eV (7.6 eV) belong to the $[Tf_2N]^-$ ion in the complex. The MO analysis shows furthermore that these states are particularly delocalized over the bis-sufonyl-amide core. The highest occupied state of the $[EMIM]^+$ ion in the complex, which is mainly localized on the π orbital of the imidiazole ring, appears at 9.1 eV (7.7 eV). This means that in the complex it is significantly shifted to lower binding energies compared to the isolated $[EMIM]^+$ ion, where we found the HOMO binding energy at 11.9 eV. This difference is obviously caused by the negative charge of the $[Tf_2N]^-$ counterion of the complex. On the other hand, for the highest occupied state of the isolated $[Tf_2N]^-$ ion, we calculated a binding energy of 3.9 eV compared to 6.7 eV (5.3 eV) in the complex. According to our calculations, the second prominent peak, located at ~11.4 eV (10.0 eV; assigned as 2pF in Figure 2), contains states attributed to the nonbonding orbitals of the fluorine atoms in the $[Tf_2N]^-$ ion. Notably, for the isolated $[Tf_2N]^-$ ion MOs of the same character are found for two states peaking the DOS at 8.2 eV, which is about the energy shift found for the HOMOs as well.

3.5. DFT Calculations of the Vibrational Structure. In order to interpret the HREELS spectra, we have calculated the vibrational DOS (Figure 4b) by DFT and analyzed the corresponding normal-modes. This enables us to interpret the HREELS spectra on a molecular level. We find good agreement between the background-corrected RT-HREELS spectrum and the calculated vibrational DOS, if we use a Gaussian-broadening of 120 cm^{-1} (FWHM). Furthermore, each mode is weighted by the respective IR- and Raman-activity in a ratio of 2:1, which emerges from the best fit of the predominantly IR-active mode at 1200 cm^{-1} and the predominantly Raman-active peak at 3090 cm^{-1}, respectively. Double-loss peaks have been taken into account as well using a weighting factor of 0.125 for the best fit of the most prominent peak at 2400 cm^{-1} (2×1200 cm^{-1}). Thus, the calculated vibrational spectra match the HREELS data qualitatively. The most pronounced vibrational structures between ~1000 and ~1400 cm^{-1} are dominated by coupled antisymmetric O═S═O and CF_3 stretching modes in the $[Tf_2N]^-$ ion (see Figure 3a peak I and II), and, indeed are found to possess the highest IR-activity. Corresponding symmetric modes, which we expect between 500 and 650 cm^{-1}, are much lower in dipole activity and consequently not resolved in the HREELS spectra.

As the low-temperature HREELS spectra reveals, the vibrational spectra of the [EMIM][Tf_2N] film are depth-dependent at 100 K. As mentioned above, spectra with high primary beam energy are basically the same as for RT (see Figure 3b peaks I−III). For the HREELS spectrum with $E_0 = 2.5$ eV, however, we need a more sophisticated way of fitting the calculated DOS to the experimental spectrum (see Figure 4c). The key to such a fit is the orientation of the dipole derivative vector of the vibrational modes and their allocation onto the two ions, the $[EMIM]^+$ and the $[Tf_2N]^-$. We found that there are normal modes with dipole derivative vector perpendicular to the imidazole ring of the $[EMIM]^+$ ion, contributing to the peaks IV and VI, which are additionally found in the low-temperature ($T = 100$ K) HREELS spectrum for $E_0 = 2.5$ eV.

4. Discussion

4.1. Electronic and Vibrational Structure at RT. As already reported previously, the VB data obtained by MIES, UPS, and XPS are rather similar and agree well with DFT calculations[14] (see Figure 4a). Thus, a variation of the information depth does not lead to significant changes in the spectra, indicating that, at room temperature, both species are present at the outermost surface without a preferential molecular orientation. In this study, this interpretation is further supported by vibrational spectroscopy (HREELS). The data presented in Figure 3 do not change significantly if the primary beam energy is varied, as far as the observed loss features are concerned. Since the probing depth is dependent on primary beam energy according to $d \propto E_0^{\sim 0.5}$ (ref 29), the presented sets of spectra illustrate the different information depth. Thus, we conclude that at room temperature the surface electronic and vibrational structure is very similar to the bulk structure.

However, the FWHM of the elastic peak is in the range of 100−500 cm^{-1} is strongly dependent on primary beam energy. In all cases it is much higher than the device resolution for the applied settings. At room temperature the FWHM decreases monotonously from 420 cm^{-1} at $E_0 = 2.5$ eV to 220 cm^{-1} at $E_0 = 80$ eV with increasing primary beam energy. At present, we are not able to give a detailed interpretation for this observation. However, a similar behavior is found for semiconductor surfaces with a depth dependent charge carrier concentration.[28,29] Similar effects might be responsible here, too. However, proof of the existence of free carriers in IL requires additional investigations related to calculations based on dielectric theory. Note, that the situation is even more complicated here, since the FWHM could also be influenced by changes in the viscosity and conductivity of the ionic liquid, especially when the temperature is varied. Consequently, the following discussion will be based solely on the observed vibrational structure.

4.2. Vibrational Structure at Low *T*. The decrease of the RT-IL film temperature has strong impact on the surface vibrational structure; the low-temperature HREELS data differ remarkably from the RT data. Especially, with low primary beam energy and high surface sensitivity, the well pronounced (CF_3 and antisymmetric O═S═O related) vibrational modes are almost absent, whereas the modes around 800 cm^{-1}, expected according to our DFT calculations, are present. The latter vibrations are associated to the imidazolium-H bending modes and to the $[Tf_2N]^-$ O═S═O symmetric stretching modes. As already pointed out, the information depth becomes larger with increasing beam energy. We observe that the spectra become increasingly similar to the RT data. This behavior may be simulated by considering a reorientation of the ion pairs in the outermost surface region. In addition, we have to take the well-known dipole selection rules (e.g., in ref 25) into account, where only those vibrations, having oscillating dipole moments perpendicular to the surface, contribute to the specular regime. In our qualitative model, we considered the reorientation of the ion pairs with the $[EMIM]^+$ ring lying flat and either the anion or the cation as the outermost group. By removing the vibrations with oscillating dipole moments parallel to the surface, we can qualitatively explain the disappearance of the modes around 1100 cm^{-1} and the appearance of the modes around 800 cm^{-1} in the HREELS spectra (Figure 4c). In addition, in the comparison of HREELS spectra and our frequency fit, the $[Tf_2N]^-$-related signatures matching the selection rules appear less pronounced but are still present. Summarizing, the temperature dependence of the HREELS spectra may be understood consistently only if changes in the molecular order close to the surface are assumed. Such changes in the molecular order should influence the valence band structure of the surface and thus result in changes of the MIES and UPS spectra. Even if other origins cannot completely ruled out, such changes at low temperatures are indeed observed as already described.

4.3. High-Temperature Results. We find a strong decrease of the intensity from both cation and anion, starting around 350 K. Upon heating, changes in the low binding energy part of the MIES and UPS spectra are observed besides the disappearance of the 2pF emission (already observed upon cooling from room temperature down to 127 K, ref 13). In UPS, emission originating from the Au substrate becomes visible. The MIES spectra differ now from the corresponding UPS data due to a change in the interaction process. Metastable He atoms now interact mainly via the Auger neutralization process, as is anticipated for a high work function metal such as Au. Thus, the appearance of the substrate emission during heating signals desorption of the material. Above 530 K, both the MIES and UPS spectra are practically identical with those of the neat Au substrate.

On the other hand, the temperature for the onset of the IL decomposition is reported to be between 727 and 742 K.[30] Thus, decomposition can be excluded as the reason for the observed intensity decrease, and our results offer a very direct proof that early volatilization of [EMIM][Tf_2N] takes place under reduced pressure. This finding lends strong support to the recent observations in refs 16, 17, and 31 of an early volatilization of [EMIM][Tf_2N] under reduced pressure. In particular, a vapor pressure of 1.24×10^{-4} Torr (as measured with the integral effusion Knudsen method at a residual pressure of 10^{-5} Torr) was reported at 455.2 K; the absence of IL decomposition during the evaporation process was established by infrared spectroscopy.[31]

5. Summary

On the basis of UPS, MIES, and HREELS, backed-up by DFT calculations, we have investigated the surface structure of the room-temperature ionic liquid [EMIM][Tf_2N] between 100 and 620 K. We found that at RT the surface structure is similar to that of the bulk. At low temperatures (below 200 K), the conductivity of the film decreases drastically. According to HREELS, the surface structure at 100 K differs remarkably from that of the bulk. The presented data lead to the conclusion that, at low temperatures, the molecules at the surface−vacuum interface are not randomly oriented anymore. For heating the sample under UHV conditions, our MIES and UPS data give evidence that volatilization of [EMIM][Tf_2N] starts around 350 K.

Acknowledgment. We are grateful to F. Endres (Clausthal University of Technology) for the supply of the RT-IL samples and his continuous interest in this work.

References and Notes

(1) Yoshimura, D.; Yokoyama, T.; Nishi, T.; Ishii, H.; Ozawa, R.; Hamaguchi, H.; Seki, K. *J. Electron Spectrosc. Relat. Phenom.* **2005**, *144−147*, 319.

(2) Wasserscheid, P.; Keim, W. *Angew. Chem.* **2000**, *112*, 3926.

(3) Binnemans, K. *Chem. Rev.* **2005**, *105*, 4148.

(4) Crosthwaite, J. M.; Muldoon, M. J.; Dixon, J. K.; Anderson, J. L.; Brennecke, J. F. *J. Chem. Thermodyn.* **2005**, *37*, 559.

(5) Endres, F.; El Abedin, S. Z. *Phys. Chem. Chem. Phys.* **2006**, *8*, 2101.

(6) Kölle, P.; Dronskowski, R. *Inorg. Chem.* **2004**, *43*, 2803.

(7) Welton, T. *Chem. Rev.* **1999**, *99*, 2071.

(8) Pinilla, C.; Del Popolo, M. G.; Lynden-Bell, R. M.; Kohanoff, J. *J. Phys. Chem. B* **2005**, *109*, 17922.

(9) Dupont, J.; Suarez, P. A. Z. *Phys. Chem. Chem. Phys.* **2006**, *8*, 2441.

(10) Caporali, S.; Bardi, U.; Lavacchi, A. *J. Electron Spectrosc. Relat. Phenom.* **2006**, *151*, 4.

(11) Smith, E. F.; Villar-Garcia, I. J.; Briggs, D.; License P. *Chem. Commun.* **2005**, 5633.

(12) Smith, E. F.; Rutten, F. J. M.; Villar-Garcia, I. J.; Briggs, D.; License, P. *Langmuir* **2006**, *22*, 9386.

(13) Höfft, O.; Bahr, S.; Himmerlich, M.; Krischok, S.; Schaefer, J. A.; Kempter, V. *Langmuir* **2006**, *22*, 7120.

(14) Krischok, S.; Öttking, R.; Beenken, W. J. D.; Himmerlich, M.; Lorenz, P.; Höfft, O.; Bahr, S.; Kempter, V.; Schaefer, J. A. *Z. Phys. Chem.* **2006**, *220*, 1407.

(15) Gottfried, J. M.; Maier, F.; Rossa, J.; Gerhard, D.; Schulz, P. S.; Wasserscheid, P.; Steinrück, H.-P. *Z. Phys. Chem.* **2006**, *220*, 1439.

(16) Rebelo, L. P. N.; Lopes, J. N. C.; Esperanca, J. M. S. S.; Filipe, E. *J. Phys. Chem. B* **2005**, *109*, 6040.

(17) Earle, M. J.; Esperanca, J. M. S. S.; Gilea, M. A.; Lopes, J. N. C.; Rebelo, L. P. N.; Magee, J. W.; Seddon, K. R.; Widegren, J. A. *Nature* **2006**, *439*, 831.

(18) Frisch, M. J.; Trucks, G. W.; Schlegel, H. B.; Scuseria, G. E.; Robb, M. A.; Cheeseman, J. R.; Montgomery, J. A., Jr.; Vreven, T.; Kudin, K. N.; Burant, J. C.; Millam, J. M.; Iyengar, S. S.; Tomasi, J.; Barone, V.; Mennucci, B.; Cossi, M.; Scalmani, G.; Rega, N.; Petersson, G. A.; Nakatsuji, H.; Hada, M.; Ehara, M.; Toyota, K.; Fukuda, R.; Hasegawa, J.; Ishida, M.; Nakajima, T.; Honda, Y.; Kitao, O.; Nakai, H.; Klene, M.; Li, X.; Knox, J. E.; Hratchian, H. P.; Cross, J. B.; Bakken, V.; Adamo, C.; Jaramillo, J.; Gomperts, R.; Stratmann, R. E.; Yazyev, O.; Austin, A. J.; Cammi, R.; Pomelli, C.; Ochterski, J. W.; Ayala, P. Y.; Morokuma, K.; Voth, G. A.; Salvador, P.; Dannenberg, J. J.; Zakrzewski, V. G.; Dapprich, S.; Daniels, A. D.; Strain, M. C.; Farkas, O.; Malick, D. K.; Rabuck, A. D.; Raghavachari, K.; Foresman, J. B.; Ortiz, J. V.; Cui, Q.; Baboul, A. G.; Clifford, S.; Cioslowski, J.; Stefanov, B. B.; Liu, G.; Liashenko, A.; Piskorz, P.; Komaromi, I.; Martin, R. L.; Fox, D. J.; Keith, T.; Al-Laham, M. A.; Peng, C. Y.; Nanayakkara, A.; Challacombe, M.; Gill, P. M. W.; Johnson, B.; Chen, W.; Wong, M. W.; Gonzalez, C.; Pople, J. A. *Gaussian 03*, revision C.02; Gaussian, Inc.: Wallingford, CT, 2004.

(19) Becke, A. D. *J. Chem. Phys.* **1993**, *98*, 5648.

(20) Janak, J. F. *Phys. Rev. B* **1978**, *18*, 7165.

(21) Politzer, P.; Abu-Awwad, F. *Theor. Chem. Acc.* **1998**, *99*, 83.

(22) Stowasser, R.; Hoffmann, R. *J. Am. Chem. Soc.* **1999**, *121*, 3414.

(23) Hamel, S.; Duffy, P.; Casida, M. E.; Salahub, D. R. *J. Electron Spectrosc. Relat. Phenom.* **2002**, *123*, 345.

(24) Zhan, C.-G.; Nichols, J. A.; Dixon, D. A. *J. Phys. Chem. A* **2003**, *107*, 4184.

(25) Ibach, H; Mills, D. L. *Electron Energy Loss Spectroscopy and Surface Vibrations*; Kluwer Academic Press: Norwell, MA, 1982.

(26) Wasserscheid, P.; Welton, T. (eds.) *Ionic Liquids in Synthesis*; Wiley-VCH: New York, 2003.

(27) Fredlake, C. P.; Crosthwaite, J. M.; Hert, D. G.; Aki, S. N. V. K.; Brennecke, J. F. *J. Chem. Eng. Data* **2004**, *49*, 954.

(28) Polyakov, V. M.; Elbe, A.; Wu, J.; Lapeyre, G. J.; Schaefer, J. A. *Appl. Surf. Sci.* **1996**, *104*−*105*, 24.

(29) Polyakov, V. M.; Elbe, A.; Schaefer, J. A. *Surf. Sci.* **1999**, *420*, 43.

(30) Huddleston, J. G.; Visser, A. E.; Reichert, W. M.; Willauer, H. D.; Broker, G. A.; Rogers, R. D. *Green Chem.* **2001**, *3*, 156.

(31) Zaitsau, D. H.; Kabo, G. J.; Strechan, A. A.; Paulechka, Y. U.; Tschersich, A.; Verevkin, S. P.; Heintz, A. *J. Phys. Chem. A.* **2006**, *110*, 7303.